High-Order Topological Pumping on a Superconducting Quantum Processor

Cheng-Lin Deng [1,2,*] Yu Liu [1,2,*] Yu-Ran Zhang [3,*] Xue-Gang Li,[4] Tao Liu [3] Chi-Tong Chen [1,2]
Tong Liu [1,2] Cong-Wei Lu,[5] Yong-Yi Wang,[1,2] Tian-Ming Li,[1,2] Cai-Ping Fang [2] Si-Yun Zhou,[2] Jia-Cheng Song [2]
Yue-Shan Xu,[1,2] Yang He,[1,2] Zheng-He Liu,[1,2] Kai-Xuan Huang [4] Zhong-Cheng Xiang,[1,2,6] Jie-Ci Wang [7]
Dong-Ning Zheng [1,2,8,9,6] Guang-Ming Xue,[4,6] Kai Xu [1,4,8,9,6,†] H. F. Yu,[4,‡] and Heng Fan [1,4,8,9,6,§]

[1]*Institute of Physics, Chinese Academy of Sciences, Beijing 100190, China*
[2]*School of Physical Sciences, University of Chinese Academy of Sciences, Beijing 100049, China*
[3]*School of Physics and Optoelectronics, South China University of Technology, Guangzhou 510640, China*
[4]*Beijing Academy of Quantum Information Sciences, Beijing 100193, China*
[5]*Department of Physics, Applied Optics Beijing Normal University, Beijing 100875, China*
[6]*Hefei National Laboratory, Hefei 230088, China*
[7]*Department of Physics and Key Laboratory of Low Dimensional Quantum Structures and Quantum Control of Ministry of Education,
Hunan Normal University, Changsha, Hunan 410081, China*
[8]*Songshan Lake Materials Laboratory, Dongguan, Guangdong 523808, China*
[9]*CAS Center for Excellence in Topological Quantum Computation, UCAS, Beijing 100190, China*

High-order topological phases of matter refer to the systems of n-dimensional bulk with the topology of m-th order, exhibiting $(n - m)$-dimensional boundary modes and can be characterized by topological pumping. Here, we experimentally demonstrate two types of second-order topological pumps, forming four 0-dimensional corner localized states on a 4×4 square lattice array of 16 superconducting qubits. The initial ground state of the system at half-filling, as a product of four identical entangled 4-qubit states, is prepared using an adiabatic scheme. During the pumping procedure, we adiabatically modulate the superlattice Bose-Hubbard Hamiltonian by precisely controlling both the hopping strengths and on-site potentials. At the half pumping period, the system evolves to a corner-localized state in a quadrupole configuration. The robustness of the second-order topological pump is also investigated by introducing different on-site disorder. Our Letter studies the topological properties of high-order topological phases from the dynamical transport picture using superconducting qubits, which would inspire further research on high-order topological phases.

Introduction—High-order symmetry-protected topological (HOSPT) phases of matter derive from the electric dipole insulators to the multipole insulators in a modern formulation of Berry phase in band structures [1,2]. The bulk-boundary correspondence for the quadrupole insulators establishes a connection between a two-dimensional bulk in a second-order topological phase and zero-dimensional topological-protected corner-localized states [3]. Recent literature reported the experiments on the HOSPT phases by observing the topologically nontrivial corner states on platforms such as photons [4–9], phonons [10–12], electric circuits [13,14], and metamaterial of microwave resonators [15–17]. However, to demonstrate quantized charge transport of the HOSPT phases remains very elusive. Recently, Ref. [18] shows that

a topological pump, e.g., the Thouless pump [19–33], can also provide a dynamical characterization of HOSPT phases, which depends on the topology of the pump cycle. Corner states appear during topological pumping on a 2D superlattice Bose-Hubbard model with staggered hopping strengths. A tuple of four Chern numbers is defined to measure quantized charge transport for the C_4-symmetric HOSPT phases [18].

Here, we experimentally demonstrate diagonal and nondiagonal HOSPT pumps on a 4×4 square lattice array of superconducting qubits. The initial ground state of the Hamiltonian at half-filling, separable as a product of four 4-qubit entangled states, is prepared using an adiabatic scheme. During the pumping process, we tune the frequencies of the couplers, connecting nearby qubits, to dynamically manipulate the hopping strengths. Together with the dynamical control of the qubits frequencies, we simulate the time-dependent Hamiltonian, enabling the implementation of a cyclic pump. During the first half pumping procedure, the system evolves from the topologically trivial
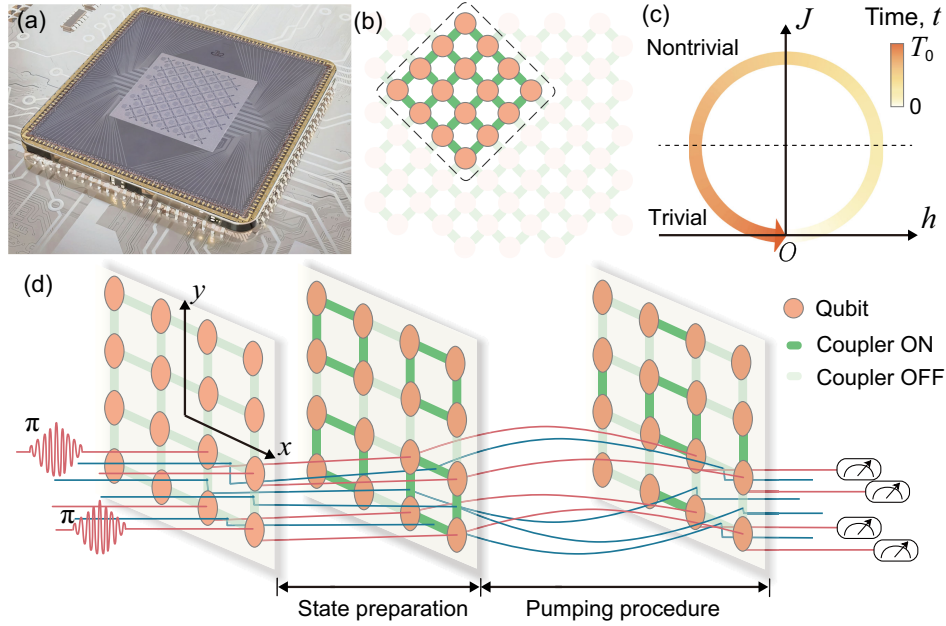

FIG. 1. Quantum processor and experimental scheme. (a) Photograph of the superconducting processor that is fabricated using the flip-chip technique. (b) Qubits array. The processor is integrated with 62 qubits and 105 couplers, forming a square lattice. A subset of 4×4 qubits and 24 couplers are used in our experiments. (c) Pumping trajectory. Parameters of the hopping strength J and the on-site potential h are dynamically modulated following a closed loop for a full pumping period. (d) Lattice configuration and experimental sequences. For each 4-qubit unit cell (down-right 4×4 block as an example), the initial ground state of the system is prepared by first exciting the diagonal two qubits to states $|1\rangle$ and then applying adiabatic controls of the frequencies of both qubits and couplers. During the pumping procedure, the system Hamiltonians evolve slowly by tuning the hopping strengths and the on-site potentials between and on qubits, respectively.

regime to the topologically nontrivial regime. At the half pumping period for both diagonal and nondiagonal pumps, the systems evolve to two different types of topological corner states, respectively. We experimentally observe the average amount of charge transport during the diagonal and nondiagonal pumps, which agree well with the anticipated fractional charge distributions [18]. We also experimentally investigate the diagonal HOSPT pump with on-site potential disorder. Our results open up the avenue for studying HOSPT pumps on various quantum-simulating platforms.

Setup and model—On our processor, a flip-chip technique is employed to integrate 62 superconducting qubits, arranged in a 2D square lattice, and to incorporate tunable couplers as lattice bonds [34], see Fig. 1(a). In our experiments, a subset of 16 qubits configured in a 4×4 square lattice is selected, see Fig. 1(b). The system can be described as the Bose-Hubbard model [35–37] with negative on-site nonlinear interactions with an average value of -260 MHz, which is much larger than the hopping strength. Thus, the system can be effectively described with hard-core bosons, which does not alter the results of our study [18,38]. The Hamiltonian under open boundary conditions (OBC) reads

$$\hat{H}^{\text{OBC}} = -\sum_{x=-D}^{D-1}\sum_{y=-D}^{D}\{[J(x)\hat{a}^{\dagger}_{x,y}\hat{a}_{x+1,y}+\text{H.c.}]+x\leftrightarrow y\}, \quad (1)$$

where $\hat{a}^{\dagger}_{x,y}$ ($\hat{a}_{x,y}$) denotes the hard-core bosonic creation (annihilation) operator. The subscript (x, y) denotes the coordinate of the qubit, with x and y both varying from -1.5 to 1.5 and $D = 1.5$, see Fig. 1(d). Here, $J(\xi)$, with $\xi \in \{x, y\}$, denotes the staggered hopping strength at the bond between nearby qubits along the x or y axis, as $J(\xi) = J_0 - J$ for $\xi \in \{-1.5, 0.5\}$, and $J(\xi) = J$ for $\xi \in \{-0.5, 1.5\}$, with $J \in [0, J_0]$.

In our experiments, we demonstrate two types of HOSPT pumps that transport charge diagonally and nondiagonally, respectively, whose Hamiltonians read

$$\hat{H}^{\text{diag}} = \hat{H}^{\text{OBC}} + h\sum_{x,y=-D}^{D}(-1)^{x+y}\hat{a}^{\dagger}_{x,y}\hat{a}_{x,y}, \quad (2)$$

$$\hat{H}^{\text{nondiag}} = \hat{H}^{\text{OBC}} - h\sum_{x,y=-D}^{D}(-1)^{x+D}\hat{a}^{\dagger}_{x,y}\hat{a}_{x,y}. \quad (3)$$

Here, J and h vary periodically with the time t as $J = J_0 \cos\lambda(t)$, $h = h_0 \sin\lambda(t)$, with $\lambda(t) = \pi - 2\pi t/T_0$, with T_0 being the pumping period. We choose the period as $T_0 = 500$ ns that is much shorter than the average qubits decoherence times $\overline{T}_1 = 17.5$ μs and $\overline{T}_2 = 2.7$ μs, see Supplemental Material [39]. We choose $J_0/2\pi = 3$,

$h_0/2\pi = 10$, $J_0'/2\pi = 3$, and $h_0'/2\pi = 3.5$ MHz for the diagonal and nondiagonal pumps, respectively.

The system has a C_4 symmetry with staggered hopping strengths. For the diagonal pump, staggered on-site potentials, $\pm h$, are applied on qubits with the same negative (positive) sign in a diagonal (off-diagonal) direction of the lattice [Fig. 3(a)]. Similarly, for the nondiagonal pump, staggered on-site potentials, $\pm h$, are applied on qubits along the x direction of the lattice, see Fig. 4(a). Both cases break the C_4 symmetry except $h = 0$. In our experiments, we prepare the initial state as the same ground state of the Hamiltonians $\hat{H}^{\mathrm{diag}}$ and $\hat{H}^{\mathrm{nondiag}}$ in Eqs. (2),(3) at $t = 0$ ns. As the Hamiltonians evolve, with J and h varying slowly along the closed trajectory as shown in Fig. 1(c), the system evolves adiabatically to topologically nontrivial phases, manifesting corner localized states at half period $t = T_0/2$, see Fig. 1(d).

Initial ground state preparation—The initial state, as the ground state of the superlattice Hamiltonians at half-filling when $t = 0$ ns, is topologically trivial. Moreover, the 4×4 lattice consists of four independent 2×2 unit cells, see Fig. 2(a). Thus, the initial ground state can be written as a product of four identical 4-qubit entangled states $|\Psi_{\mathrm{ini}}\rangle = |\psi_{\mathrm{tgt}}\rangle^{\otimes 4}$ with

$$|\psi_{\mathrm{tgt}}\rangle = \frac{1}{\sqrt{8}}\left(\left|\begin{matrix}00\\11\end{matrix}\right\rangle + \left|\begin{matrix}10\\10\end{matrix}\right\rangle + \left|\begin{matrix}11\\00\end{matrix}\right\rangle + \left|\begin{matrix}01\\01\end{matrix}\right\rangle\right)$$
$$+ \frac{1}{2}\left(\left|\begin{matrix}01\\10\end{matrix}\right\rangle + \left|\begin{matrix}10\\01\end{matrix}\right\rangle\right). \qquad (4)$$

Notably, the initial state satisfies a particle-hole symmetry at half-filling, resulting in an additional Z_2 symmetry in addition to C_4 symmetry.

In our experiments, we employ an adiabatic scheme to prepare the required 4-qubit entangled state for each unit cell independently. The procedures for all 4 unit cells are conducted in parallel, while the couplers connecting different unit cells are turned off. For each unit cell, we excite two qubits located at the off-diagonal sites, using two π-pulses transforming $|0\rangle$ to $|1\rangle$, see Fig. 2(a). Then, we gradually tune the frequencies of these two qubits from -21 MHz to the resonant frequency 0 MHz, and the hopping strengths between qubits inside each unit cell are tuned from 0 to 6 MHz adiabatically, see Fig. 2(a). The fidelity of the prepared 4-qubit state ρ_{exp} of each unit cell, compared with the target state $\rho_{\mathrm{tgt}} \equiv |\psi_{\mathrm{tgt}}\rangle\langle\psi_{\mathrm{tgt}}|$, is defined as $F(\rho_{\mathrm{tgt}}, \rho_{\mathrm{exp}}) = \mathrm{tr}(\rho_{\mathrm{tgt}}^{1/2}\rho_{\mathrm{exp}}\rho_{\mathrm{tgt}}^{1/2})^{1/2}$ [46]. The density matrices of ρ_{exp} are obtained by performing quantum state tomography (QST) measurements at different times [46,47], which are presented in Fig. 2(b1)–2(b3) and compared with the target state in Fig. 2(c). The fidelity versus the preparation time is plotted in Fig. 2(d), and the optimal fidelity of the prepared state for each unit cell
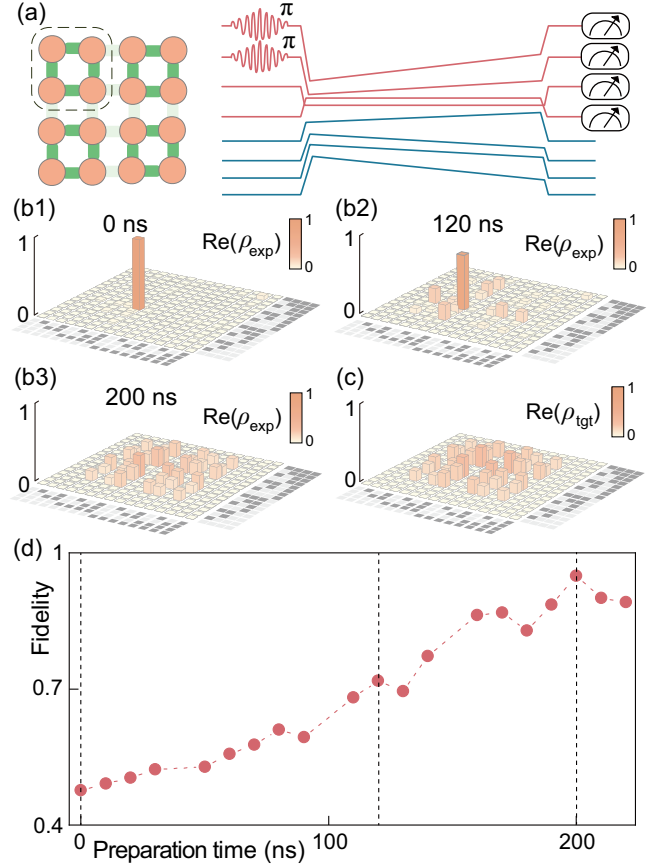

FIG. 2. Initial ground state preparation. (a) 16-qubit lattice and pulse sequences on a 4-qubit unit cell. Two off-diagonal qubits are excited to $|1\rangle$ with two π pulses. Then, the 4-qubit entangled state is prepared by adiabatically controlling the frequencies of both qubits and couplers. (b1)–(b3) 4-qubit density matrices ρ_{exp}, measured by quantum state tomography at different evolution times. (c) 4-qubit density matrix ρ_{tgt} of the reduced target state in Eq. (4). (d) Fidelity of the evolving 4-qubit state versus the preparation time, compared with the target state.

achieves 94.9% at 200 ns. More details are presented in Supplemental Material [39].

Diagonal and nondiagonal HOSPT pumping—After the initial state preparation, we simultaneously tune the on-site potentials and the hopping strengths along the cyclic pumping trajectory on the J–h plane, through the Z-control lines of the qubits and the couplers, respectively. Thus, the systems undergo approximately adiabatic evolutions. During the first half pumping period, the systems evolve from topologically trivial phases to topologically non-trivial phases, as illustrated in Fig. 1(c). Furthermore, at the half pumping period $t = 250$ ns, the corner localized states appear.

During the full pumping procedure, we measure all 16 qubits in the $\{|0\rangle, |1\rangle\}$ basis with 6000 single-shot readouts every 10 ns, and the excitation probabilities of all 16 qubits P_1 for the diagonal second-order topological pump are plotted in Fig. 3(c) versus the evolution time t and
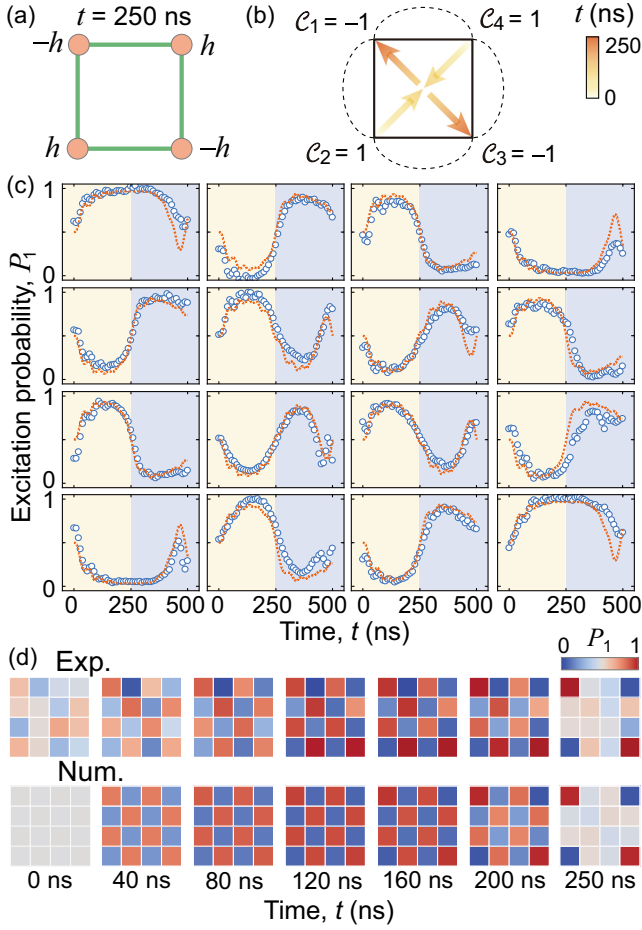
FIG. 3. Diagonal HOSPT pumping. (a) Additional on-site potentials for diagonal HOSPT pumping. (b) Chern number tuples for diagonal HOSPT pumping, and each Chern number $\mathcal{C}_{1,2,3,4}$ is associated with the charge transport current from the off-diagonal corners to the diagonal corners. (c) Time evolutions of the measured excitation probabilities P_1 for all 16 qubits (blue circles) during the full pumping period from $t = 0$ to 500 ns, which are compared with the numerical simulations (red dotted curves). (d) Measured excitation probabilities P_1 for all 16 qubits at different evolution times, which are compared with numerical simulations. At the half pumping period $t = 250$ ns, four corner states are observed.

compared with the numerical results. At the half pumping period $t = 250$ ns, the corner localized states clearly appear, see Figs. 3(d) and 4(c) for the diagonal and non-diagonal pumps, respectively. The experimental results are compared with numerical simulations using the same experimental parameters.

Because of the bulk-boundary correspondence, a tuple of Chern numbers $\mathcal{C}_{1,2,3,4}$ can be introduced under corner-periodic boundary conditions (CPBCs) [18]. At the half pumping period, the amount of the transport charge at each corner Δq_i is related to the Chern number as

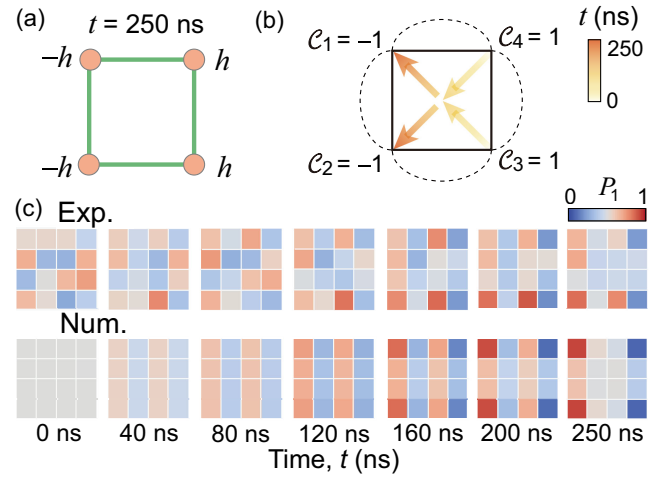$$\Delta q_i = -\mathcal{C}_i/2, \tag{5}$$

FIG. 4. Nondiagonal HOSPT pumping. (a) Additional on-site potentials for nondiagonal HOSPT pumping. (b) Chern number tuples for nondiagonal HOSPT pumping, and each Chern number $\mathcal{C}_{1,2,3,4}$ is associated with the charge transport current from the right-side corners to the left-side corners. (c) Measured excitation probabilities P_1 for all 16 qubits at different evolution times, compared with numerical simulations. At the half pumping period $t = 250$ ns, four corner states are observed.

which is obtained by measuring the change of the excitation probability $\Delta P_1^{(i)}$ at each corner $i \in \{1, 2, 3, 4\}$. Since $\mathcal{C}_{1,2,3,4}^{\text{diag}} = (-1, 1, -1, 1)$ for the diagonal pump and $\mathcal{C}_{1,2,3,4}^{\text{nondiag}} = (-1, -1, 1, 1)$ for the nondiagonal one, the average corner transport charge $\Delta q = \sum_{i=1}^{4} |\Delta q_i|/2 = 1$. Here, we obtain that $\Delta q = 0.964$ and 0.555 for the diagonal and the nondiagonal second-order topological pumps, respectively, which are compared with 0.985 and 0.836 from the numerical simulation. The experimental results for the diagonal pump agree well with the theoretical expectations, and the imperfections may result from the accuracy of the experimental control on J and h, decoherence, and the inconformity of the qubits on the processor. Nevertheless, the non-diagonal HOSPT pump requires a much longer pumping period to fulfill the adiabatic condition, see Supplemental Material [39] for more details.

Robustness of HOSPT pumping in the presence of disorder—Next, we investigate the effects of on-site potential disorder on diagonal HOSPT pumping. Here, on-site potential disorder $h = h_0 \sin \lambda(t) + \delta h$, we apply on each qubit, following a uniform distribution $\delta h \in [-W, W]$, with W being the disorder strength. The disorder strength $W/2\pi$ ranges from 0 to 40 MHz, and for each disorder strength, 40 different configurations of the disorder are applied to obtain the average amount of transport charge $\overline{\Delta q}$. Figure 5(a) shows the average amount of transport charge $\overline{\Delta q}$ versus the disorder strength W, which is compared with numerical simulations using the experimental parameters. The $\overline{\Delta q}$ first decreases slightly, as $W/2\pi$ increases from 0 MHz, and then decreases intensely, as $W/2\pi \gtrsim 10$ MHz.
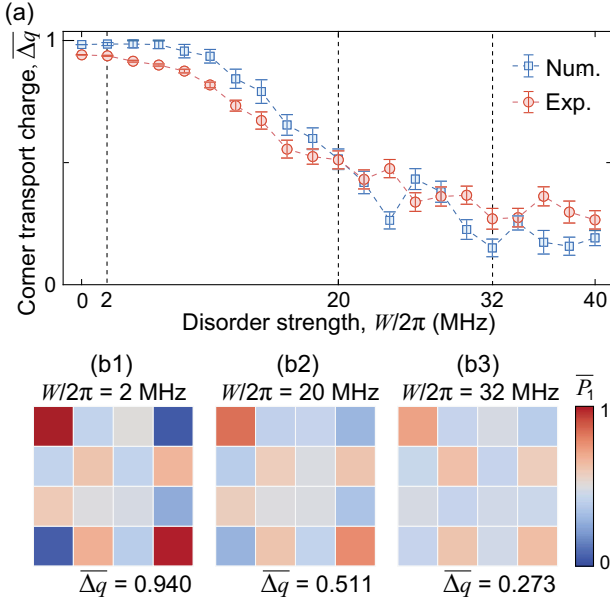
FIG. 5. (a) The average amount of transport charge $\overline{\Delta q}$ for diagonal HOSPT pumping versus the disorder strength ranging from $W/2\pi = 0$ to 40 MHz. (b1)–(b3) Measured average excitation probabilities $\overline{P_1}$ for all 16 qubits at the half pumping period with different disorder strengths $W/2\pi = 2$, 20, and 32 MHz with respect to $\overline{\Delta q} = 0.940$, 0.511, and 0.273, respectively.

When $W/2\pi \gtrsim 40$ MHz, $\overline{\Delta q}$ tends to be zero, indicating that the quantized pump seems to disappear. The effects of on-site disorder on the corner-localized states can be observed from the average excitation probabilities $\overline{P_1}$ of all 16 qubits at the half pumping period $t = 250$ ns, which are shown in Figs. 5(b1)–5(b3) for different disorder strengths. Our experimental results confirm the robust topological protection of the zero-dimension corner state in topological pumping and are in good agreement with numerical simulations [48].

Conclusion and discussion—We have experimentally demonstrated the diagonal and nondiagonal HOSPT pumps on a square-lattice array of 16 superconducting qubits, with accurate dynamical modulations of the hopping strengths and on-site potentials between and on qubits, respectively. The HOSPT corner states are observed at the half-pumping period, of which the robustness is investigated by introducing on-site disorder. The ground state of the studied Hamiltonian at half-filling is with a Hilbert space dimension scaling exponentially with the number of qubits, which is entangled and has experimental challenges. The time evolution of the system may involve hard conventional computation, leading to a quantum computational advantage problem [49]. Another interesting issue is to detect the non-local quantum correlations, e.g., string order parameters [50] and entanglement entropy [51], during the pumping procedures. Our Letter would inspire further studies on various HOSPT phases and topological pumps

on different quantum-simulating platforms with a larger system size [50–52].

[1] W. A. Benalcazar, B. A. Bernevig, and T. L. Hughes, Quantized electric multipole insulators, Science **357**, 61 (2017).

[2] R. Resta, Quantum-mechanical position operator in extended systems, Phys. Rev. Lett. **80**, 1800 (1998).

[3] R. Citro and M. Aidelsburger, Thouless pumping and topology, Nat. Rev. Phys. **5**, 87 (2023).

[4] W. A. Benalcazar, J. Noh, M. Wang, S. Huang, K. P. Chen, and M. C. Rechtsman, Higher-order topological pumping and its observation in photonic lattices, Phys. Rev. B **105**, 195129 (2022).

[5] S. Mittal, V. V. Orre, G. Zhu, M. A. Gorlach, A. Poddubny, and M. Hafezi, Photonic quadrupole topological phases, Nat. Photonics **13**, 692 (2019).

[6] O. Zilberberg, S. Huang, J. Guglielmon, M. Wang, K. P. Chen, Y. E. Kraus, and M. C. Rechtsman, Photonic topological boundary pumping as a probe of 4D quantum Hall physics, Nature (London) **553**, 59 (2018).

[7] Z. Wang, Y. Chong, J. D. Joannopoulos, and M. Soljačić, Observation of unidirectional backscattering-immune topological electromagnetic states, Nature (London) **461**, 772 (2009).

[8] M. Hafezi, S. Mittal, J. Fan, A. Migdall, and J. Taylor, Imaging topological edge states in silicon photonics, Nat. Photonics **7**, 1001 (2013).

[9] M. C. Rechtsman, J. M. Zeuner, Y. Plotnik, Y. Lumer, D. Podolsky, F. Dreisow, S. Nolte, M. Segev, and A. Szameit, Photonic Floquet topological insulators, Nature (London) **496**, 196 (2013).

[10] L. M. Nash, D. Kleckner, A. Read, V. Vitelli, A. M. Turner, and W. T. Irvine, Topological mechanics of gyroscopic metamaterials, Proc. Natl. Acad. Sci. U.S.A. **112**, 14495 (2015).

[11] R. Süsstrunk and S. D. Huber, Observation of phononic helical edge states in a mechanical topological insulator, Science **349**, 47 (2015).

[12] M. Serra-Garcia, V. Peri, R. Süsstrunk, O. R. Bilal, T. Larsen, L. G. Villanueva, and S. D. Huber, Observation of a phononic quadrupole topological insulator, Nature (London) **555**, 342 (2018).

[13] J. Ningyuan, C. Owens, A. Sommer, D. Schuster, and J. Simon, Time-and site-resolved dynamics in a topological circuit, Phys. Rev. X **5**, 021031 (2015).

[14] J. Bao, D. Zou, W. Zhang, W. He, H. Sun, and X. Zhang, Topoelectrical circuit octupole insulator with topologically protected corner states, Phys. Rev. B **100**, 201406(R) (2019).

[15] C. W. Peterson, W. A. Benalcazar, T. L. Hughes, and G. Bahl, A quantized microwave quadrupole insulator with topologically protected corner states, Nature (London) **555**, 346 (2018).

[16] X. Ni, M. Li, M. Weiner, A. Alù, and A. B. Khanikaev, Demonstration of a quantized acoustic octupole topological insulator, Nat. Commun. **11**, 2108 (2020).

[17] S. Imhof, C. Berger, F. Bayer, J. Brehm, L. W. Molenkamp, T. Kiessling, F. Schindler, C. H. Lee, M. Greiter, T. Neupert et al., Topolectrical-circuit realization of topological corner modes, Nat. Phys. **14**, 925 (2018).

[18] J. F. Wienand, F. Horn, M. Aidelsburger, J. Bibo, and F. Grusdt, Thouless pumps and bulk-boundary correspondence in higher-order symmetry-protected topological phases, Phys. Rev. Lett. **128**, 246602 (2022).

[19] D. J. Thouless, Quantization of particle transport, Phys. Rev. B **27**, 6083 (1983).

[20] Q. Niu and D. Thouless, Quantised adiabatic charge transport in the presence of substrate disorder and many-body interaction, J. Phys. A **17**, 2453 (1984).

[21] S. Nakajima, T. Tomita, S. Taie, T. Ichinose, H. Ozawa, L. Wang, M. Troyer, and Y. Takahashi, Topological Thouless pumping of ultracold fermions, Nat. Phys. **12**, 296 (2016).

[22] M. Lohse, C. Schweizer, O. Zilberberg, M. Aidelsburger, and I. Bloch, A Thouless quantum pump with ultracold bosonic atoms in an optical superlattice, Nat. Phys. **12**, 350 (2016).

[23] M. Lohse, C. Schweizer, H. M. Price, O. Zilberberg, and I. Bloch, Exploring 4D quantum Hall physics with a 2D topological charge pump, Nature (London) **553**, 55 (2018).

[24] O. Zilberberg, S. Huang, J. Guglielmon, M. Wang, K. P. Chen, Y. E. Kraus, and M. C. Rechtsman, Photonic topological boundary pumping as a probe of 4D quantum Hall physics, Nature (London) **553**, 59 (2018).

[25] A. Cerjan, M. Wang, S. Huang, K. P. Chen, and M. C. Rechtsman, Thouless pumping in disordered photonic systems, Light Sci. Appl. **9**, 178 (2020).

[26] S. Nakajima, N. Takei, K. Sakuma, Y. Kuno, P. Marra, and Y. Takahashi, Competition and interplay between topology and quasi-periodic disorder in Thouless pumping of ultracold atoms, Nat. Phys. **17**, 844 (2021).

[27] W. Kao, K.-Y. Li, K.-Y. Lin, S. Gopalakrishnan, and B. L. Lev, Topological pumping of a 1D dipolar gas into strongly correlated prethermal states, Science **371**, 296 (2021).

[28] M. Jürgensen, S. Mukherjee, and M. C. Rechtsman, Quantized nonlinear Thouless pumping, Nature (London) **596**, 63 (2021).

[29] W. A. Benalcazar, J. Noh, M. Wang, S. Huang, K. P. Chen, and M. C. Rechtsman, Higher-order topological pumping and its observation in photonic lattices, Phys. Rev. B **105**, 195129 (2022).

[30] Z. Tao et al., Interaction-induced topological pumping in a solid-state quantum system, arXiv:2303.04582.

[31] A.-S. Walter, Z. Zhu, M. Gächter, J. Minguzzi, S. Roschinski, K. Sandholzer, K. Viebahn, and T. Esslinger, Quantization and its breakdown in a Hubbard–Thouless pump, Nat. Phys. **19**, 1471 (2023).

[32] Z.-C. Xiang, K. Huang, Y.-R. Zhang, T. Liu, Y.-H. Shi, C.-L. Deng, T. Liu, H. Li, G.-H. Liang, Z.-Y. Mei, H. Yu, G. Xue, Y. Tian, X. Song, Z.-B. Liu, K. Xu, D. Zheng, F. Nori, and H. Fan, Simulating Chern insulators on a superconducting quantum processor, Nat. Commun. **14**, 5433 (2023).

[33] Y. Liu et al., Disorder-induced topological pumping on a superconducting quantum processor, arXiv:2401.01530.

[34] X.-G. Li, H.-K. Xu, J.-H. Wang, L.-Z. Tang, D.-W. Zhang, C.-H. Yang, T. Su, C.-L. Wang, Z.-Y. Mi, W.-J. Sun et al., Mapping a topology-disorder phase diagram with a quantum simulator, arXiv:2301.12138.

[35] Y. You, J. Bibo, and F. Pollmann, Higher-order entanglement and many-body invariants for higher-order topological phases, Phys. Rev. Res. **2**, 033192 (2020).

[36] J. Bibo, I. Lovas, Y. You, F. Grusdt, and F. Pollmann, Fractional corner charges in a two-dimensional superlattice Bose-Hubbard model, Phys. Rev. B **102**, 041126(R) (2020).

[37] F. Grusdt, M. Höning, and M. Fleischhauer, Topological edge states in the one-dimensional superlattice Bose-Hubbard model, Phys. Rev. Lett. **110**, 260405 (2013).

[38] Z. Yan, Y.-R. Zhang, M. Gong, Y. Wu, Y. Zheng, S. Li, C. Wang, F. Liang, J. Lin, Y. Xu et al., Strongly correlated quantum walks with a 12-qubit superconducting processor, Science **364**, 753 (2019).

[39] See Supplemental Material at http://link.aps.org/supplemental/10.1103/PhysRevLett.133.140402 which includes Refs. [40–45] for the information on device design, experimental methods, and additional discussion.

[40] W. A. Benalcazar, B. A. Bernevig, and T. L. Hughes, Electric multipole moments, topological multipole moment pumping, and chiral hinge states in crystalline insulators, Phys. Rev. B **96**, 245115 (2017).

[41] J. Johansson, P. Nation, and F. Nori, QuTiP: An open-source python framework for the dynamics of open quantum systems, Comput. Phys. Commun. **183**, 1760 (2012).

[42] S. Krinner, S. Storz, P. Kurpiers, P. Magnard, J. Heinsoo, R. Keller, J. Lütolf, C. Eichler, and A. Wallraff, Engineering cryogenic setups for 100-qubit scale superconducting circuit systems, Eur. Phys. J. Quantum Technol. **6**, 2 (2019).

[43] P. Krantz, M. Kjaergaard, F. Yan, T. P. Orlando, S. Gustavsson, and W. D. Oliver, A quantum engineer's guide to superconducting qubits, Appl. Phys. Rev. **6**, 021318 (2019).

[44] E. M. Purcell, H. C. Torrey, and R. V. Pound, Resonance absorption by nuclear magnetic moments in a solid, Phys. Rev. **69**, 37 (1946).

[45] F. Yan, P. Krantz, Y. Sung, M. Kjaergaard, D. L. Campbell, T. P. Orlando, S. Gustavsson, and W. D. Oliver, Tunable coupling scheme for implementing high-fidelity two-qubit gates, Phys. Rev. Appl. **10**, 054062 (2018).

[46] M. A. Nielsen and I. L. Chuang, Quantum Computation and Quantum Information (Cambridge University Press, Cambridge, England, 2010).

[47] R. Barends et al., Digitized adiabatic quantum computing with a superconducting circuit, Nature (London) **534**, 222 (2016).

[48] C. Lu, Z.-F. Cai, M. Zhang, H. Wang, Q. Ai, and T. Liu, Effects of disorder on Thouless pumping in higher-order topological insulators, Phys. Rev. B **107**, 165403 (2023).

[49] F. Arute, K. Arya, R. Babbush, D. Bacon, J. C. Bardin, R. Barends, R. Biswas, S. Boixo, F. G. Brandao, D. A. Buell *et al.*, Quantum supremacy using a programmable super-conducting processor, Nature (London) **574**, 505 (2019).

[50] G. Semeghini, H. Levine, A. Keesling, S. Ebadi, T. T. Wang, D. Bluvstein, R. Verresen, H. Pichler, M. Kalinowski, R. Samajdar, A. Omran, S. Sachdev, A. Vishwanath, M. Greiner, V. Vuletic, and M. D. Lukin, Probing topological spin liquids on a programmable quantum simulator, Science **374**, 1242 (2021).

[51] K. J. Satzinger *et al.*, Realizing topologically ordered states on a quantum processor, Science **374**, 1237 (2021).

[52] P. Sompet, S. Hirthe, D. Bourgund, T. Chalopin, J. Bibo, J. Koepsell, P. Bojović, R. Verresen, F. Pollmann, G. Salomon, C. Gross, T. A. Hilker, and I. Bloch, Realizing the symmetry-protected Haldane phase in Fermi-Hubbard ladders, Nature (London) **606**, 484 (2022).